Electronic Supplementary Material (ESI) for Physical Chemistry Chemical Physics.

Supplementary Information

Plasma-assisted defect engineering of N-doped $NiCo_2O_4$ for efficient oxygen reduction

Jingxuan Zheng, Xiangfeng Peng, and Zhao Wang*

Table S1 The ratios of Ni^{2+} / Ni^{3+} , Co^{2+} / Co^{3+} and $O_{(V/M-O)}$ determined by XPS

	Ni^{2+}/ Ni^{3+}	Co^{2+}/ Co^{3+}	$O_{(V/M-O)}$
NCO-CP-O	0.47	1.53	0.78
NCO-CP-Air	0.42	1.92	0.82

Table S2 Specific surface area of the prepared NCO-C, NCO-CP-O, NCO-CP-Air, NCO-CP-Ar catalysts

	NCO-C	NCO-CP-O	NCO-CP-Air	NCO-CP-Ar
S_{BET} (m^2 g^{-1})	12. 499	14. 986	15. 958	21. 2486

Table S3 The amount of nitrogen on samples determined by XPS

Sample	NCO-CP-AH	NCO-CP-AB	NCO-CP-AC
N %	2.02	7.45	10.10

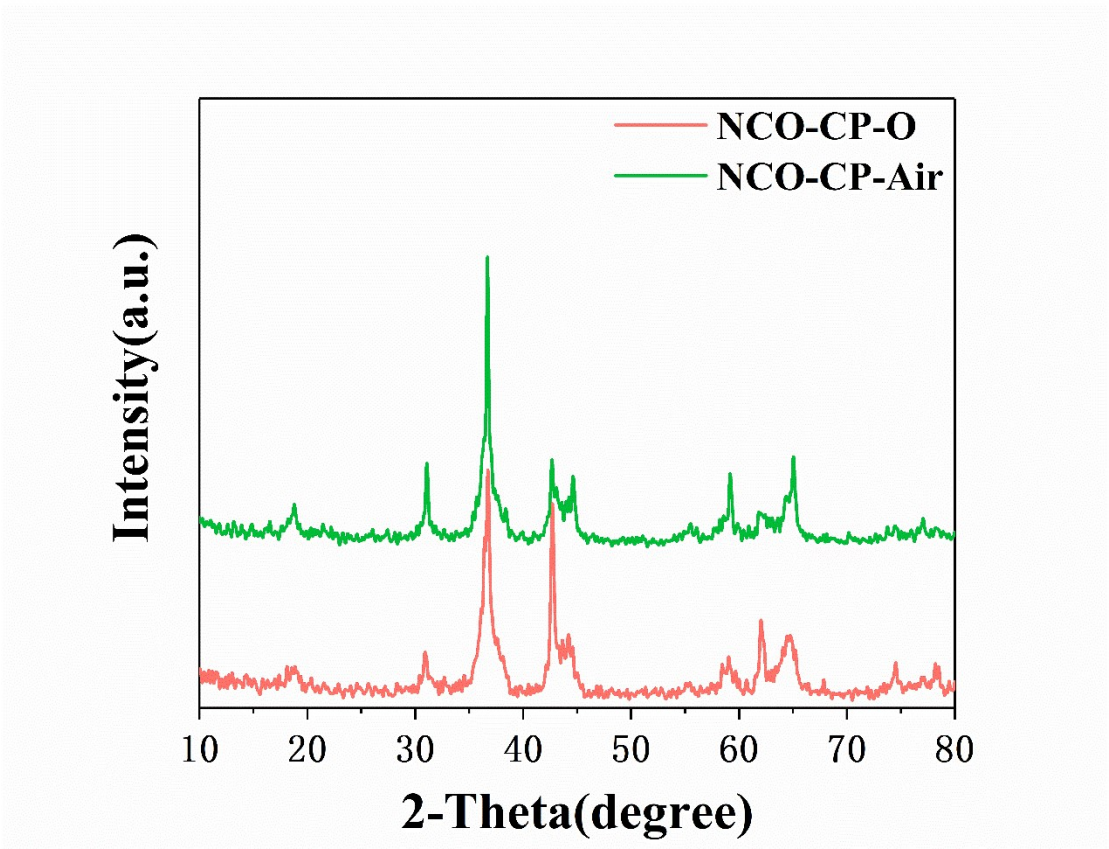

Figure S1. XRD pattern of NCO-CP-O and NCO-CP-Air

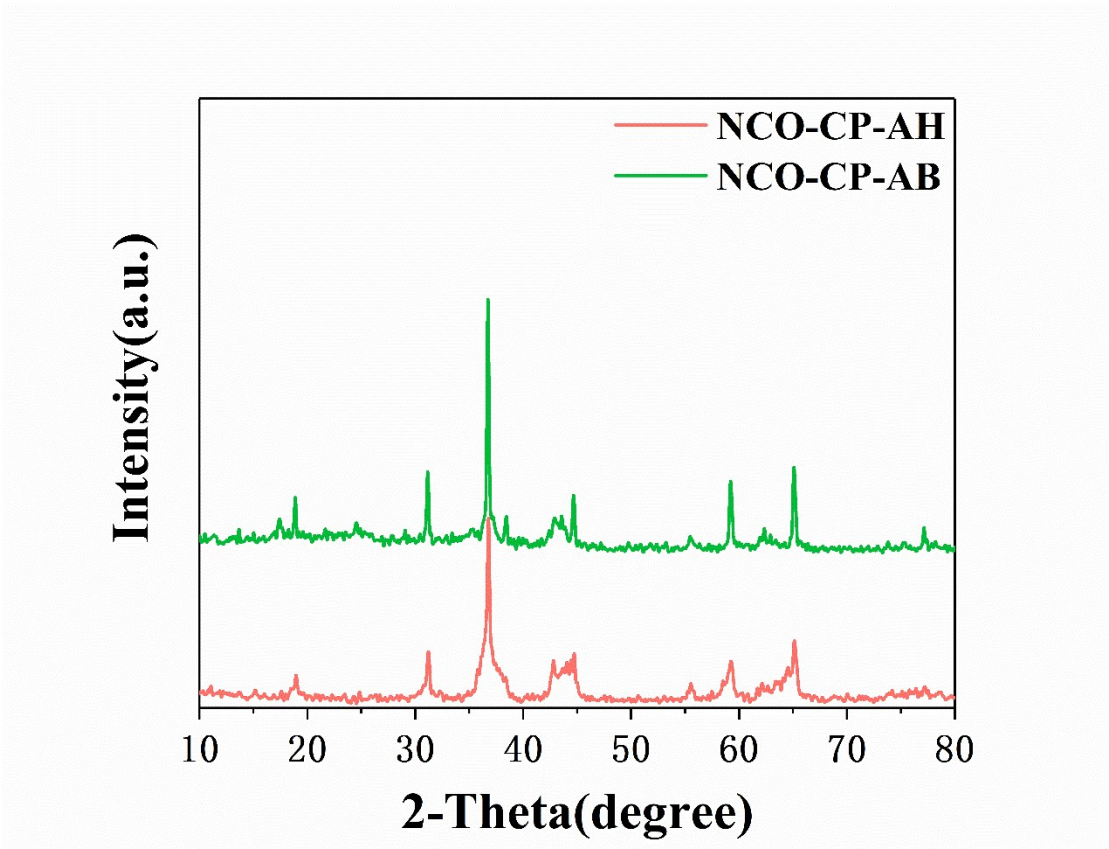

Figure S2. XRD pattern of NCO-CP-AH and NCO-CP-AB

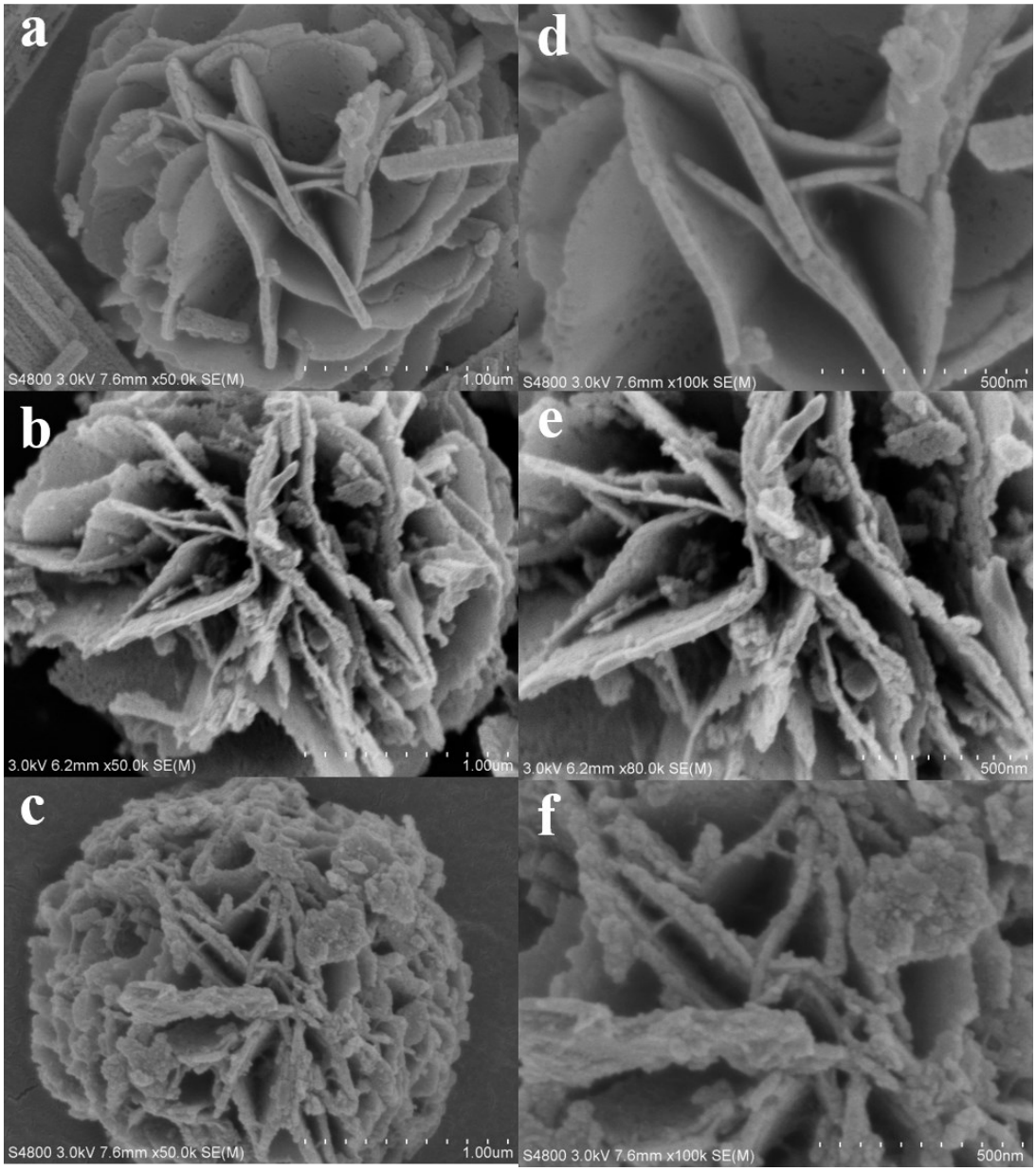

Figure S3. SEM images of the samples. **a, d**. NCO–C. **b, e**. NCO–CP–Ar. **c,f**. NCO–CP–AC.

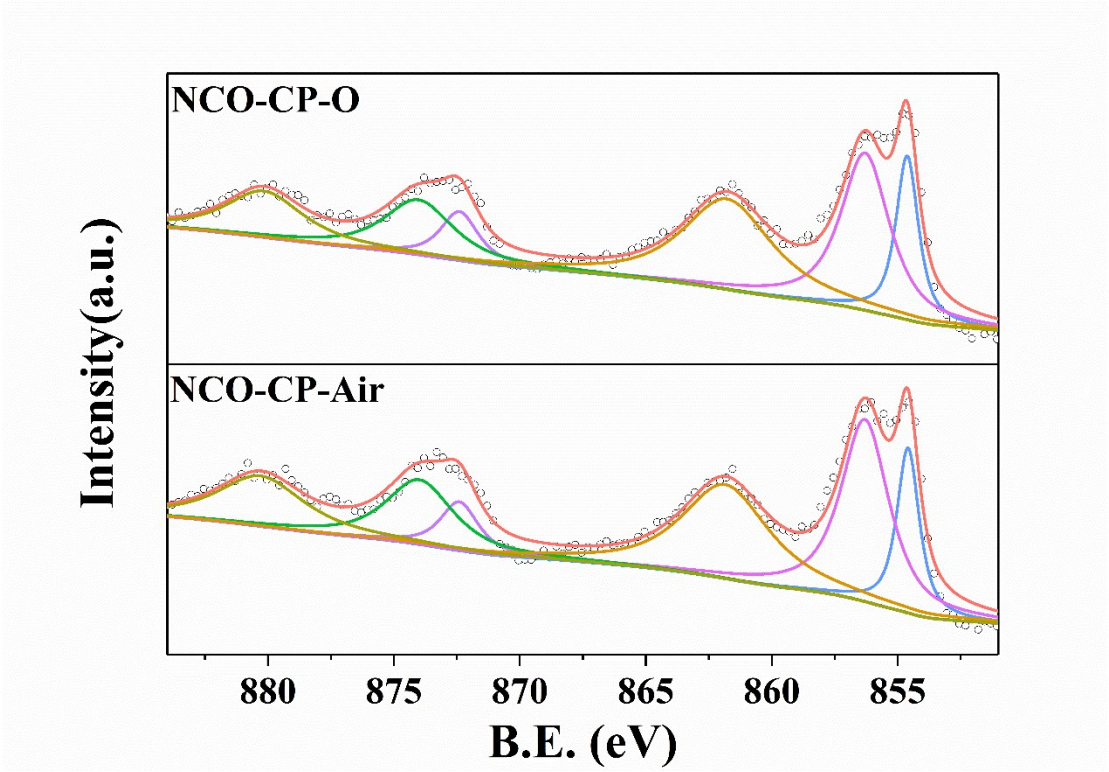

Figure S4. Deconvoluted XPS of Ni 2p of NCO-CP-O and NCO-CP-Air.

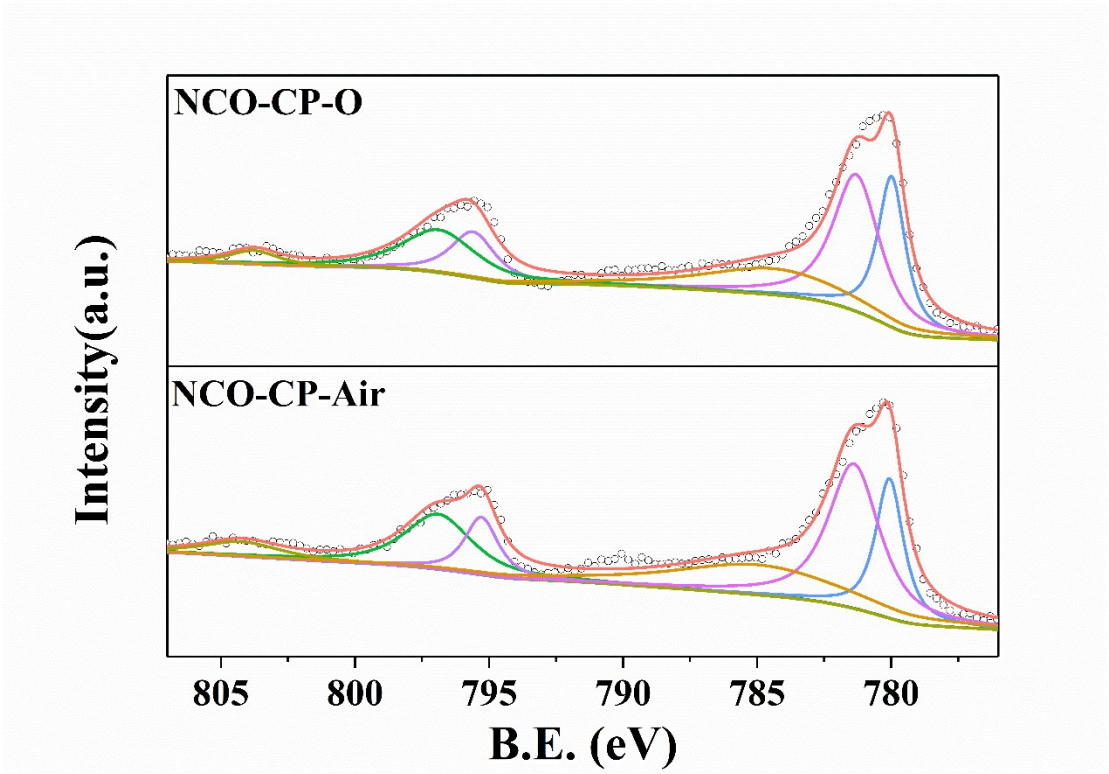

Figure S5. Deconvoluted XPS of Co 2p of NCO-CP-O and NCO-CP-Air.

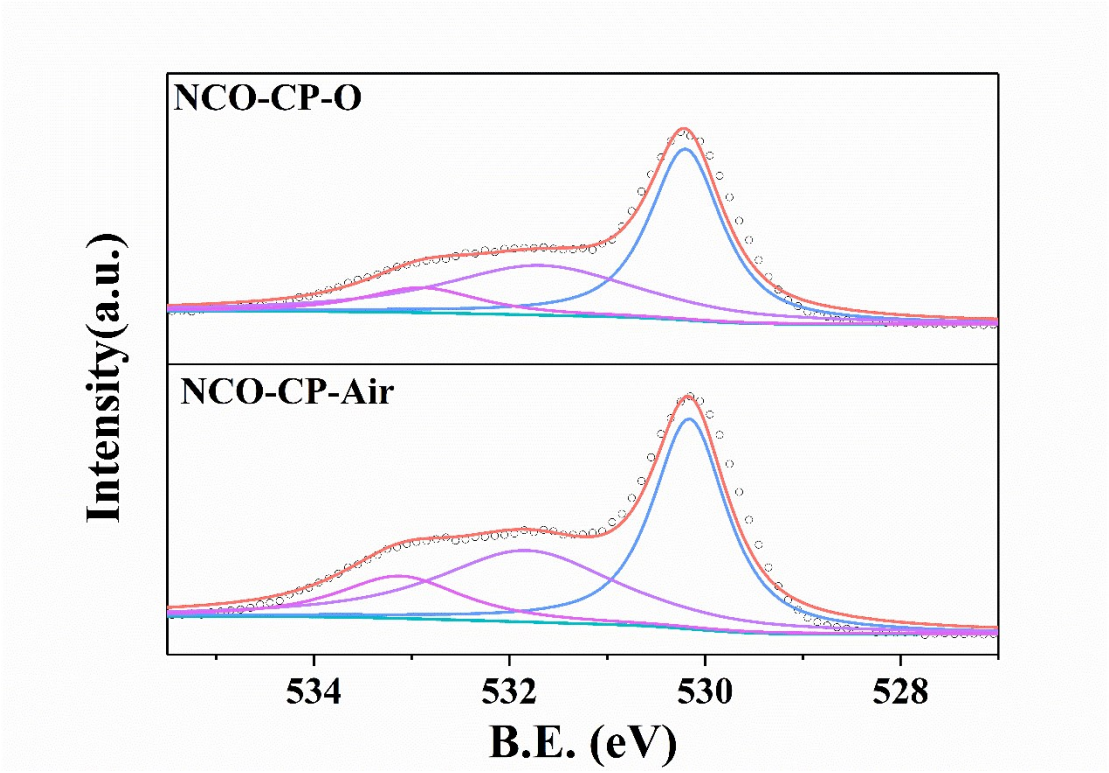

Figure S6. Deconvoluted XPS of O 1s of NCO-CP-O and NCO-CP-Air.

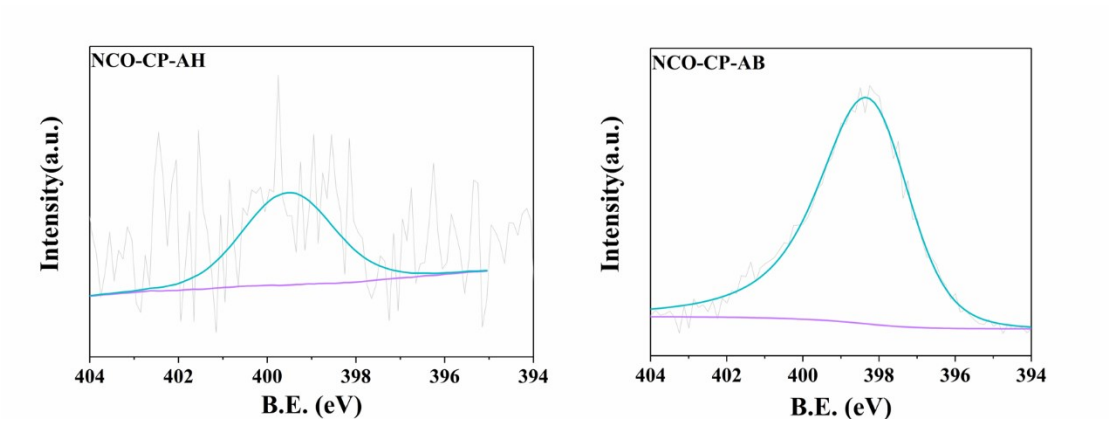

Figure S7. XPS of N 1s of NCO-CP-AH and NCO-CP-AB.

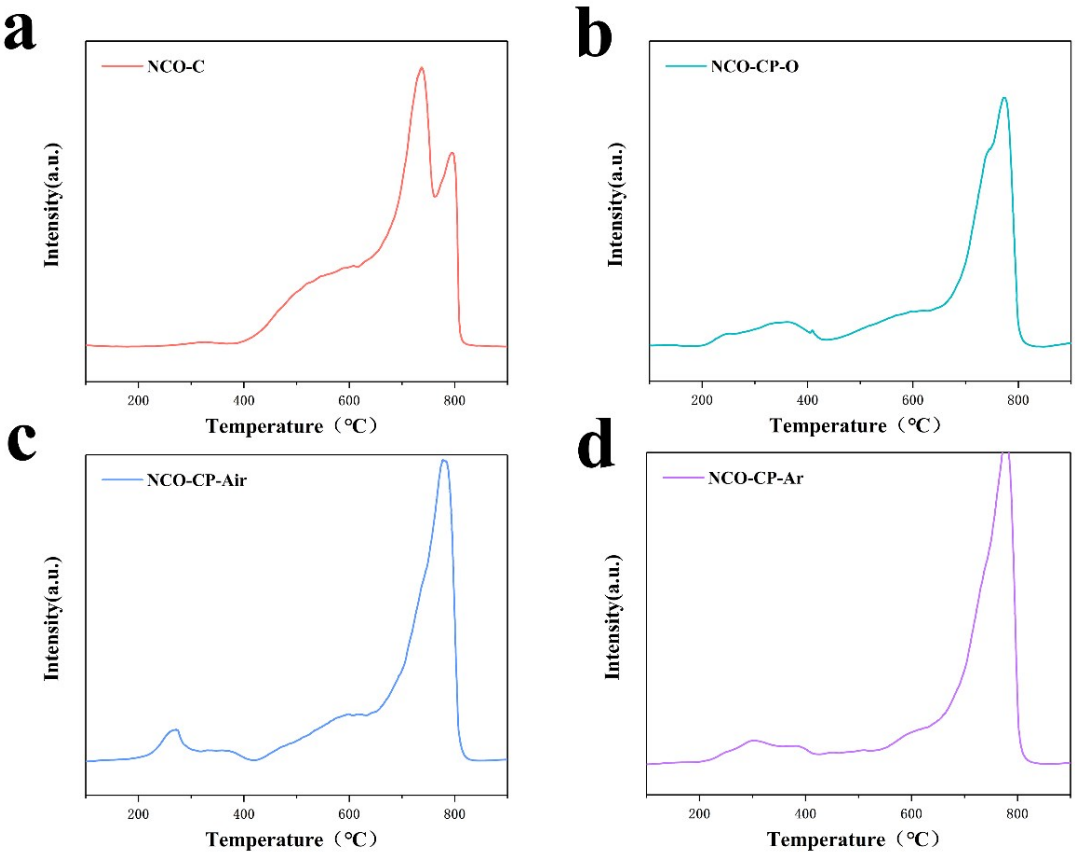

Figure S8. O_2-TPD profiles of the NCO-C, NCO-CP-O, NCO-CP-Air and NCO-CP-Ar samples.

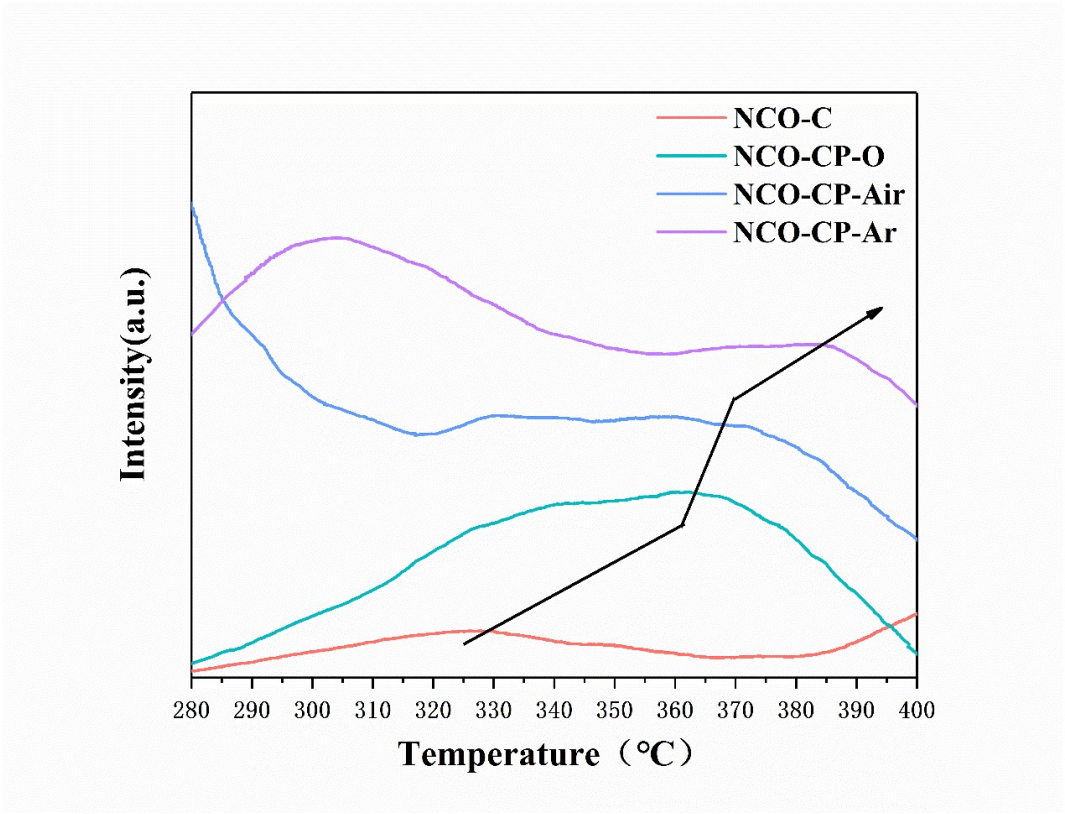

Figure S9. larger scale of O_2-TPD in 200 to 400 ℃

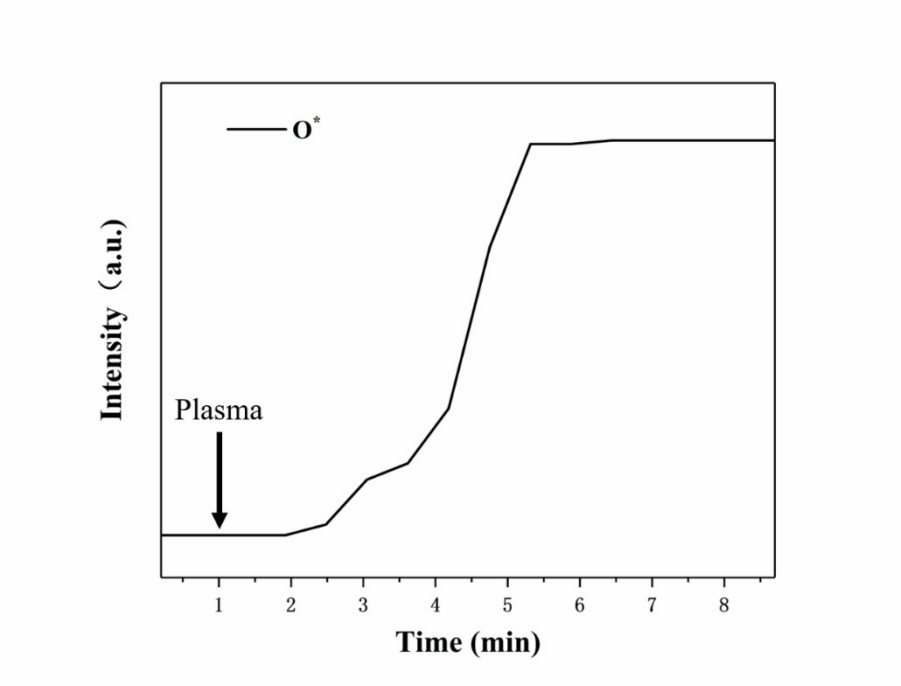

Figure S10. Mass spectrum during cold plasma treatment process of $NiCo_2O_4$.

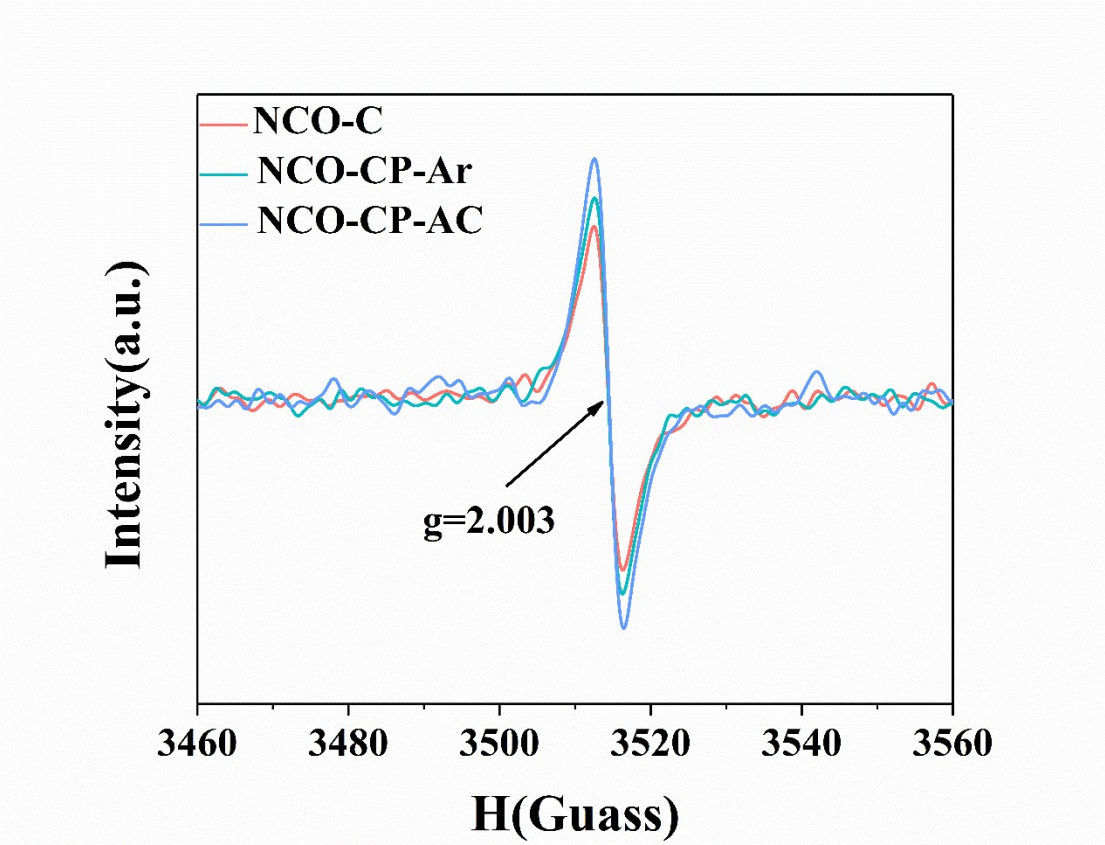

Figure S11. Electron paramagnetic resonance (EPR) spectra of NCO-C, NCO-CP-Ar and NCO-CP-AC

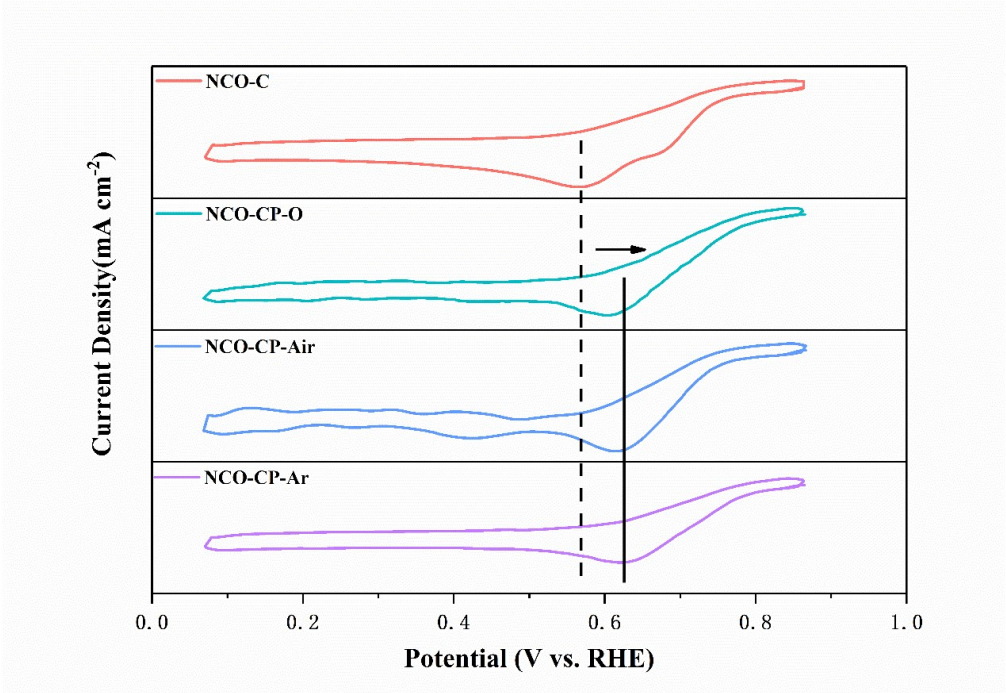

Figure S12. CV curves of NCO-C, NCO-CP-O, NCO-CP-Air and NCO-CP-Ar for ORR in O_2 saturated 0.1M KOH electrolyte with a scan rate of 10 mV s^{-1}.

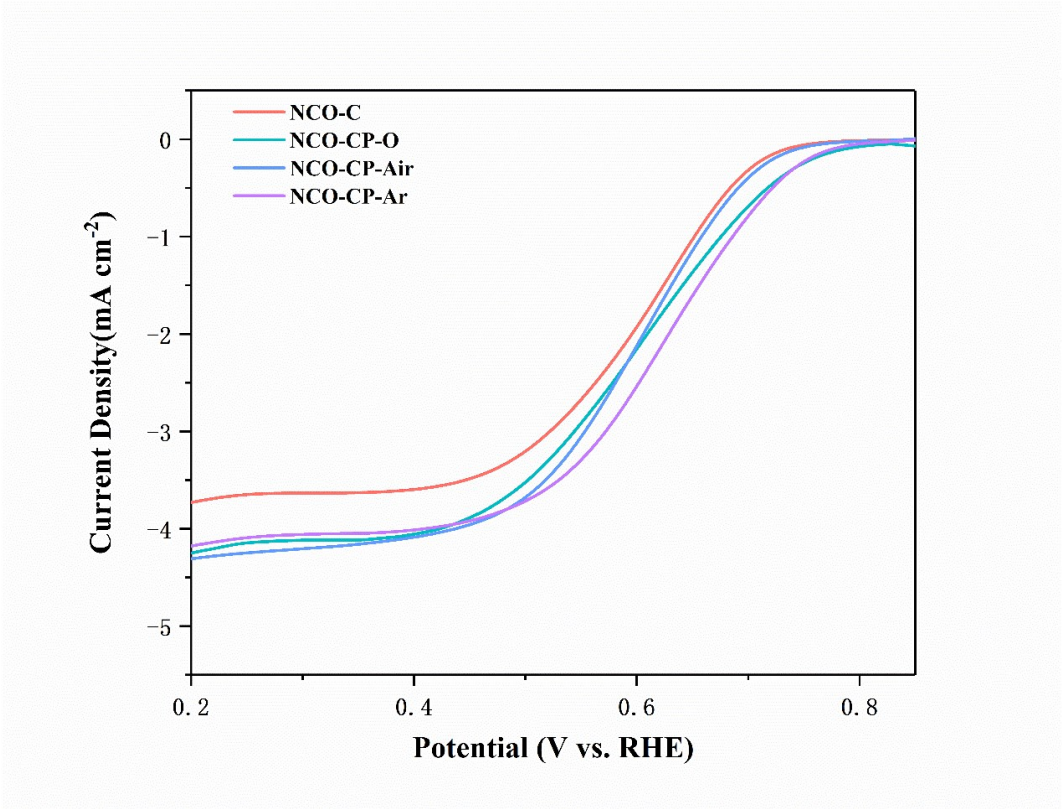

Figure S13. Linear sweep voltammetric curves of NCO-C, NCO-CP-O, NCO-CP-Air and NCO-CP-Ar for ORR at a rotating speed of 1600 rpm.

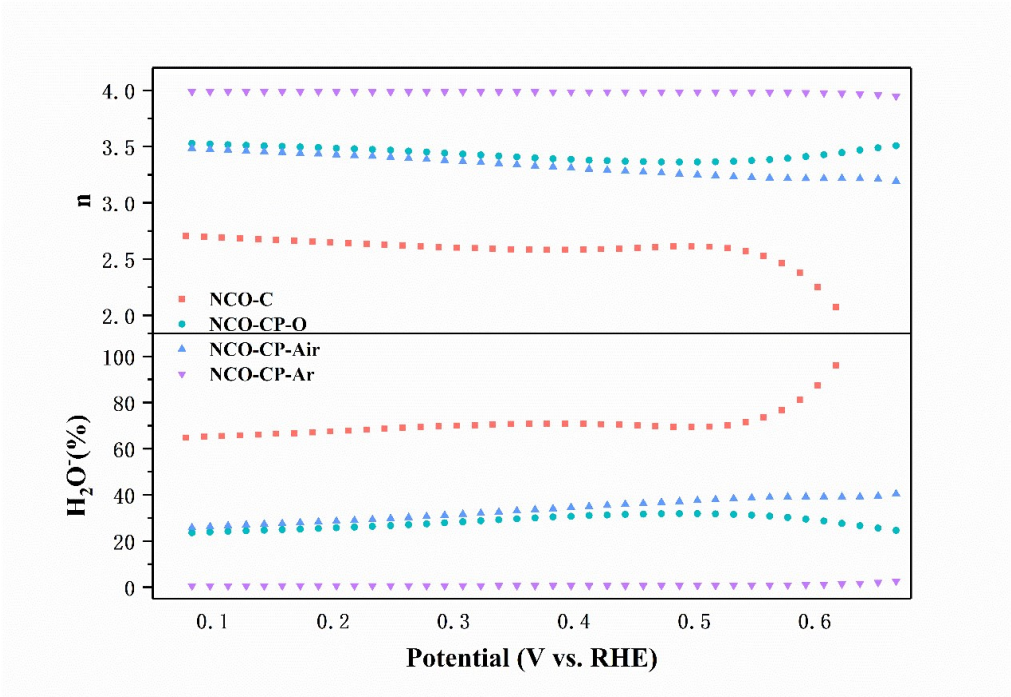

Figure S14. The electron transfer number n and peroxide (HO_2^-) yields of NCO-C,

NCO-CP-O, NCO-CP-Air and NCO-CP-Ar with respect to the total oxygen reduction products.

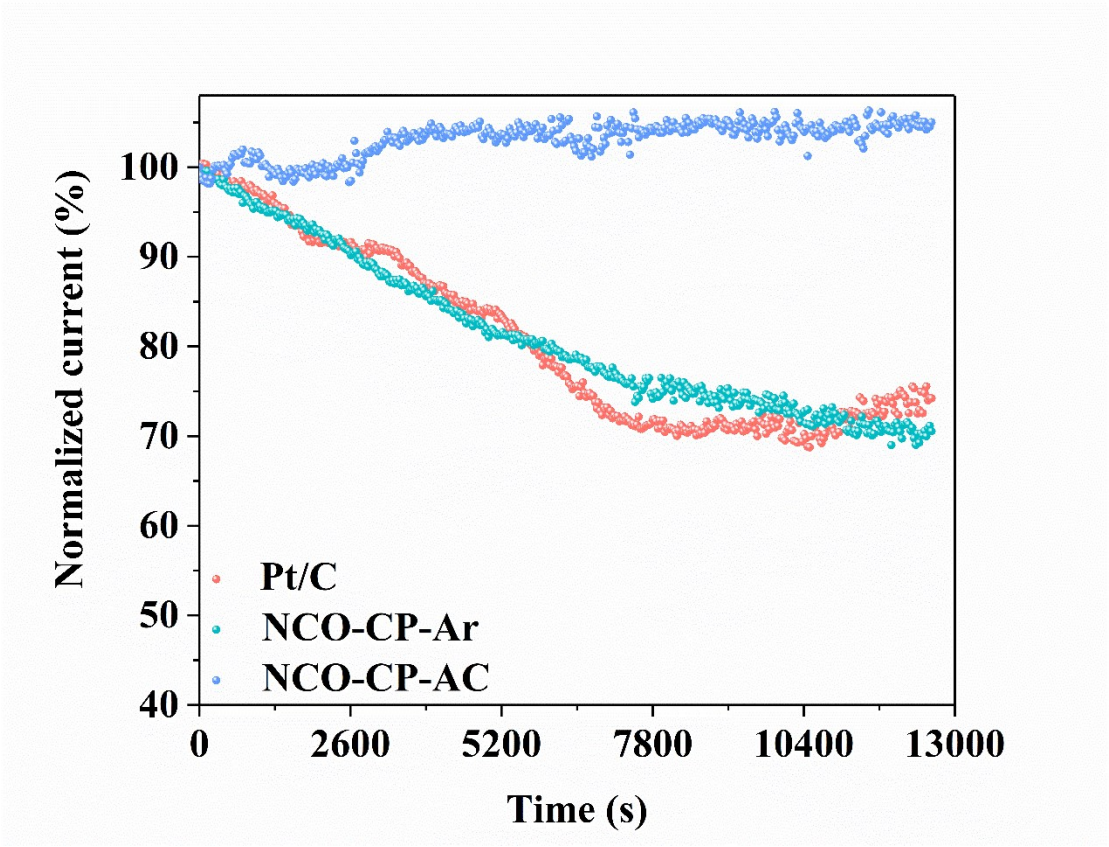

Figure S15. Stability of Pt/C, NCO-CP-Ar and NCO-CP-AC at 0.27 V vs RHE.

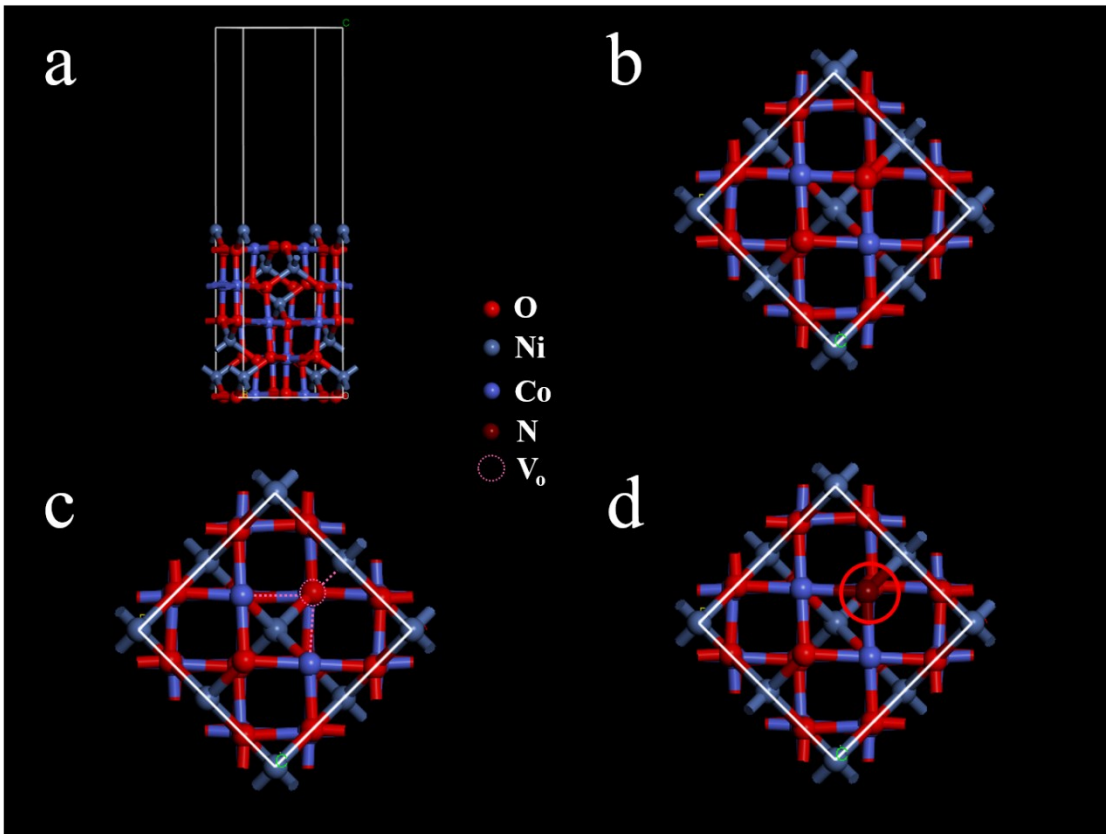

Figure S16. a, b Top and side views of NCO-C model. c, d Side views of NCO-CP-Ar and NCO-CP-AC model.

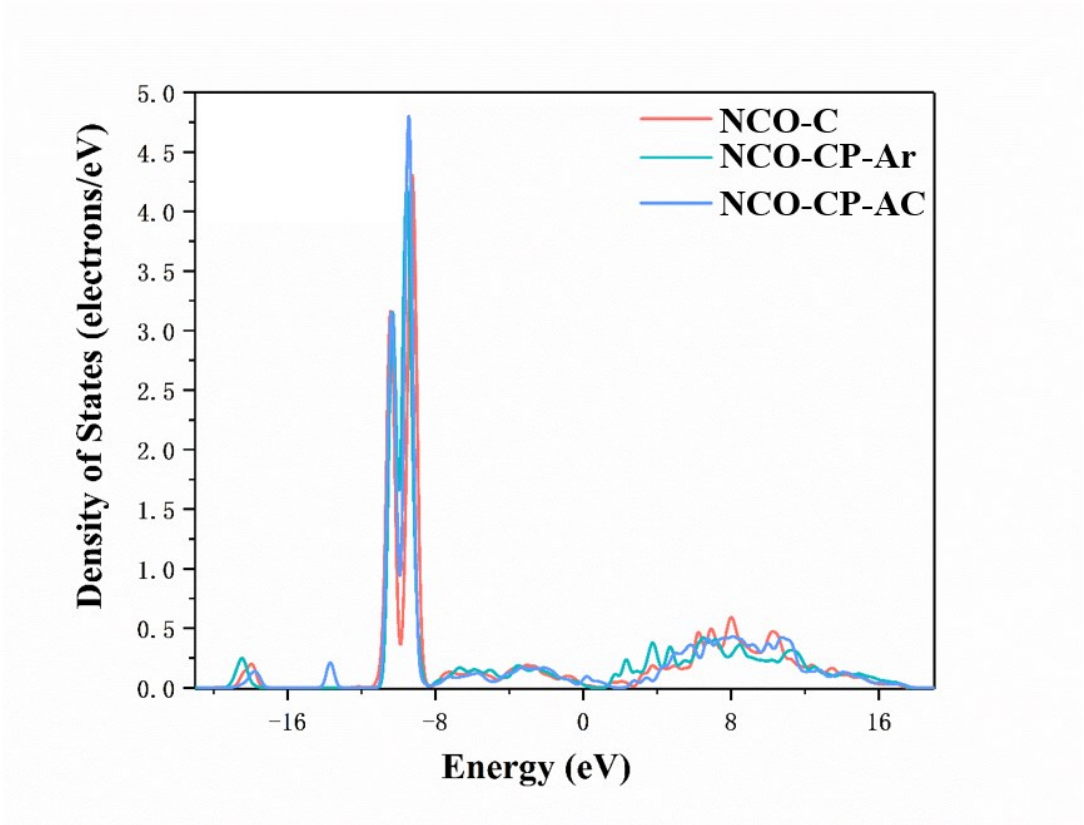

Figure S17. Computed density of states of Ni for NCO-C, NCO-CP-Ar and NCO-CP-AC.

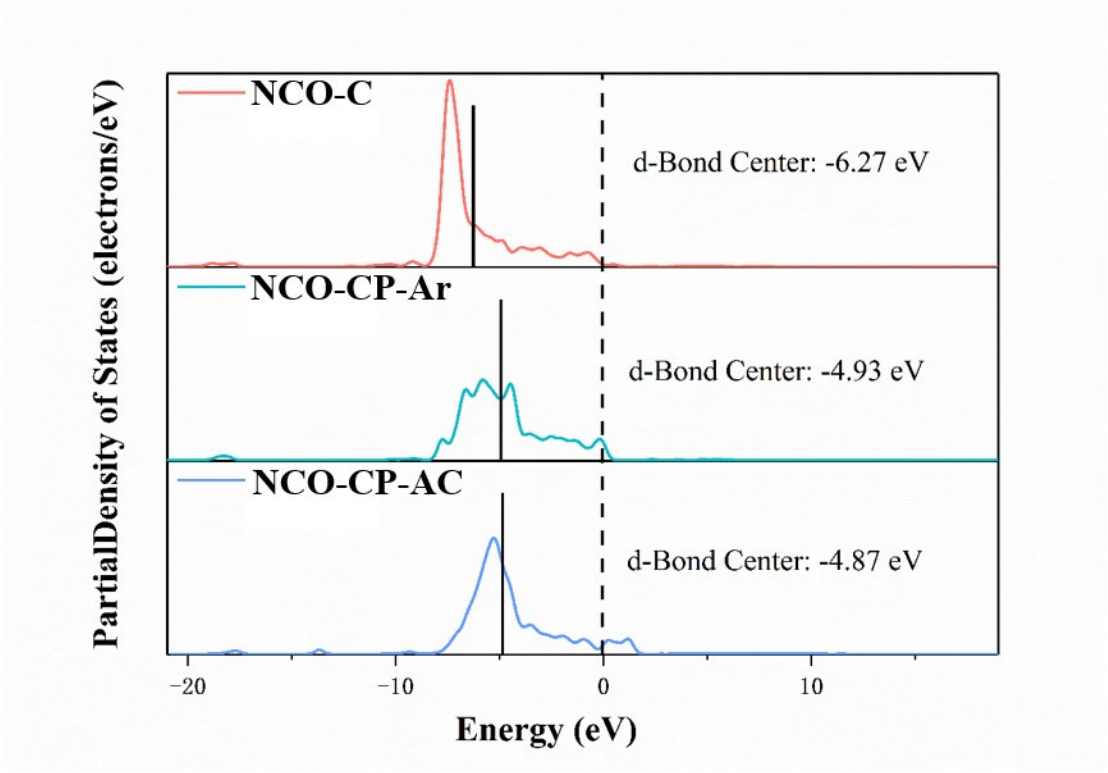

Figure S18. Computed d-bond center for NCO-C, NCO-CP-Ar and NCO-CP-AC, respectively.

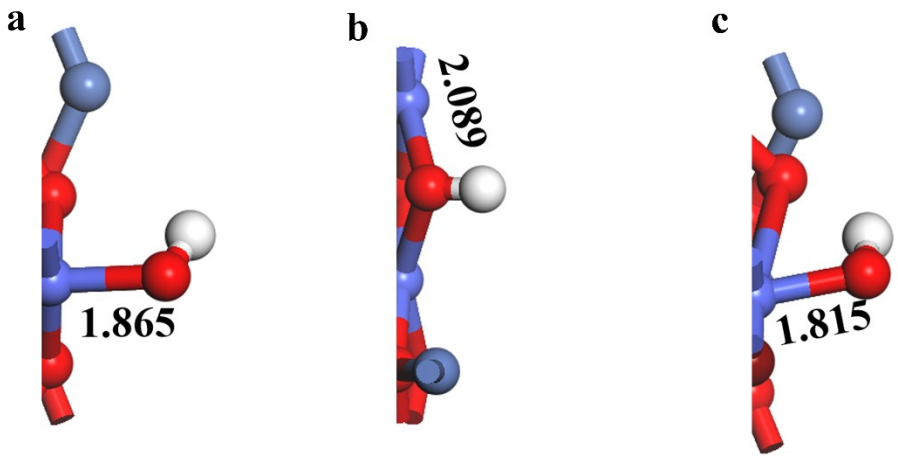

Figure S19. The structural optimizational processes of OH^- adsorbed on NCO-C, NCO-CP-Ar and NCO-CP-AC, respectively.